ChemCatChem

Research Article
doi.org/10.1002/cctc.202500847

Chemistry Europe
European Chemical Societies Publishing

www.chemcatchem.org

Ribosomal Incorporation of Thioxanthone as a Noncanonical Amino Acid Facilitates the Engineering of Photoenzymes

Marco Seifert,[a, b] Martin Termathe,*[b, c] Luca Nardo,[d] and Matthias Höhne*[b]

Photocatalysis in biocatalytic systems provides a promising approach for achieving selective and efficient chemical transformations under mild conditions. Naturally occurring photoactive cofactors are rare. To overcome this limitation, genetic code engineering can be applied to equip proteins with additional functionalities beyond those known in the 20 canonical amino acids. Here, we report the engineering of an aminoacyl-tRNA synthetase (thioXRS) that allows the incorporation of a thioxanthone-bearing noncanonical amino acid (thioX). As proof-of-concept, we utilized the versatile biocatalyst LmrR as a protein scaffold. We identified an active variant able to catalyze the *E*/*Z*-photoisomerization of a cinnamate ester derivative into coumarin. The reaction design allows direct monitoring through fluorescence measurements, as the fluorescent substrate is converted into a non-fluorescent product. This work demonstrates that thioXRS is a versatile tool for the future development of new-to-nature photoenzymes, expanding the synthetic capabilities of biocatalysis towards light-driven transformations.

1. Introduction

Nature harbors an astonishing variety of biocatalysts, yet many chemical transformations desired by chemists have no direct equivalent in natural pathways. These limitations can be overcome by repurposing existing enzymes to catalyze non-natural reactions and employing protein engineering tools to unlock novel mechanistic pathways not yet seen in nature.

Recently, enzyme catalysis was expanded into the field of photochemical transformations and photoredox catalysis, introducing a unique activation mode for initiating reactions within proteins. Light serves as an ideal high-energy "reagent", generating reactive intermediates that can otherwise be accessed only via very harsh or toxic reagents and conditions. These high-energy, open shell intermediates then undergo transformation that complement classical polar or two-electron transfer mechanisms, enabling access to complex molecular architectures, such as four-membered ring systems.[1]

Organisms utilize photocatalysis in fundamental biological processes including water splitting to generate redox equivalents for CO_2 assimilation or the repair of sunlight-induced DNA damages. However, the flavine-dependent fatty acid photodecarboxylase[2] (*Cv*FAP) remains the only natural photoenzyme that has been extensively studied and engineered for biocatalytic applications.[3–8] Beyond its role in synthesizing biofuels,[9] natural gas,[3] or ethylbenzene,[10] a key discovery was that the chiral environment surrounding the photoactive cofactor in its active site can impose stereoselectivity on the reaction.[5,6]

To expand the repertoire of photoenzymes available for biocatalysis, different approaches have been investigated. First, the potential of photoactive cofactors such as flavins or nicotinamides was explored to induce light-dependent promiscuous reactions.[1,11–13] In this approach, substrates analogs—structurally resembling the enzyme's natural ligands but lacking the functional group typically converted—bind to the active site and remain inert under dark conditions. Upon irradiation, these bound substrates undergo photoreactions initiated by the excited cofactor rather than the standard enzymatic conversion.

Second, protein scaffolds were equipped with photoactive complexes of metal ions such as iridium, nickel, and cerium[14–17] or organic photosensitizers,[18–22] which are anchored within the protein scaffold via direct binding, chelation, or bioconjugation.

One elegant approach is the direct incorporation of photocatalytic moieties as noncanonical amino acids (ncAAs) by ribosomal synthesis. This strategy allows precise positioning of the photoactive group within the protein scaffold, eliminating the need for additional derivatization steps. Genetic code expansion through stop codon suppression is a well-established technique that provides protein engineers access to a library of over 200 ncAAs for the introduction of novel functionalities.[23]

[a] *M. Seifert*
Institut für Biochemie, Universität Greifswald, Felix-Hausdorff-Straße 4, 17489, Greifswald, Germany

[b] *M. Seifert, Dr. M. Termathe, Prof. Dr. M. Höhne*
Institut für Chemie, Technische Universität Berlin, Müller-Breslau-Straße 10, 10623, Berlin, Germany
E-mail: martin.termathe@uk-essen.de
matthias.hoehne@tu-berlin.de

[c] *Dr. M. Termathe*
Research Center One Health Ruhr, Dept. Metabolism, Senescence and Autophagy, Virchowstr. 171, 45147, Essen, Germany

[d] *Dr. L. Nardo*
Como Lake Institute of Photonics, Dipartimento di Scienza e Alta Tecnologia, Università degli Studi dell'Insubria, Via Valleggio 11, Como 22100, Italy

Marco Seifert and Martin Termathe contributed equally to this work.

Supporting information for this article is available on the WWW under https://doi.org/10.1002/cctc.202500847

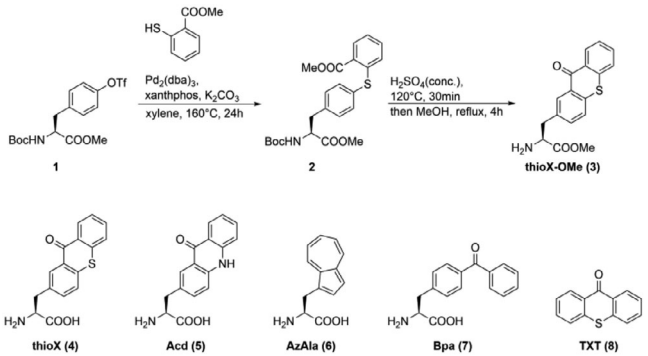

Figure 1. Chemical synthesis of the thioxanthonylalanine methyl ester (thioX-OMe, **3**) and comparison of its chemical structure with thioxanthone **8** (TXT) and other noncanonical (photoactive) amino acids. Acd – acridone-2-yl-alanine (**5**), AzAla – β-(1-azulenyl)-alanine (**6**), Bpa – benzoylphenylalanine (**7**).

Benzoylphenylalanine (Bpa) is such an example, originally developed for photo-crosslinking applications, but recently shown to facilitate [2 + 2] photocyclizations.[18,24]

To further expand the synthetic capabilities of photoenzymes, we envisioned the incorporation of a thioxanthone-bearing amino acid. Thioxanthone (TXT) offers key advantages including excitation by visible light and a long-lived triplet state. Beyond energy transfer (EnT), it can also enable photoreactions via single-electron transfer (SET) and hydrogen atom transfer (HAT) mechanisms.[25]

Achieving this goal requires (i) synthesizing an amino acid containing a thioxanthone moiety in its side chain, (ii) engineering an aminoacyl-tRNA synthetase (aaRS) capable of charging a tRNA for amber stop codon recoding, and (iii) demonstrating its integration into a model protein that can catalyze a non-natural photoreaction.

As a model system, we selected the *Lactococcus lactis* multidrug resistance regulator LmrR, which has served as a versatile scaffold for the installation of artificial catalytic functionalities in recent years.[26] LmrR bears a central hydrophobic cavity (~1400 Å^3) and due to its intrinsic flexibility, can accommodate various medium- to large-sized guest molecules, including DNA-intercalators like ethidium bromide and diverse antibiotics.

In this study, we engineered an aaRS that accepts thioxanthonylalanine and facilitates its incorporation into LmrR. We demonstrate that the modified protein catalyzes a non-natural, light-driven *E*/*Z* isomerization, providing proof of concept for the creation of a novel photoenzymatic activity.

2. Results and Discussion

2.1. Synthesis of thioX

We chemically synthesized the methyl ester derivative of thioxanthonylalanine (thioX-OMe, **3**) (see Figure 1). The protected tyrosine derivative **1** was coupled to *o*-thiosalicylate methyl ester leading to the biaryl thioether **2** with a moderate yield (38%). An intramolecular Friedel-Crafts acylation then afforded the cyclic product thioX (**4**). Initial attempts furnished the free carboxylic acid **4** with only moderate yield and purity. However, this thioX preparation was sufficient to perform our initial screening experiments. To optimize the synthesis procedure and to overcome the solubility issues of **4**, we produced the methyl ester derivative **3** (thioX-OMe) by adding a final Fischer esterification step (see Figure 1) with a good yield (81%). This derivatization allowed the facile work-up of the ncAA by liquid-liquid extraction. Ester derivatives of ncAAs have been described to facilitate cellular uptake and show increased bioavailability.[27,28] Once inside the cell, the amino acid ester undergoes hydrolysis and is thereby retained intracellularly. However, the precise mechanism and the responsible enzyme activity still needs to be elucidated.[29]

2.2. Engineering and Characterization of the thioXRS

To incorporate thioX by ribosomal synthesis, we were seeking a promiscuous aaRS with a homologous substrate scope as a starting point for our engineering efforts. Therefore, among others, we investigated the capability of the acridone-accepting synthetase AcdRS A9. This engineered Tyrosyl-RS from *Methanocaldococcus jannaschii* is the improved variant of a promiscuous aaRS (AcdRS1/G2), which incorporates acridone (Acd, **5**),[30–32] a structural analog of thioX that has served as versatile fluorescent probe for studying protein interactions and conformational changes.[30,33]

We assessed the suppression efficiency of AcdRS using a well-established super folder green fluorescence protein reporter (sfGFP_S2TAG), in which an amber stop codon (TAG) replaces the serine codon at position 2. The presence of a loaded $tRNA_{CUA}$ allows the readthrough, generating a functional sfGFP whose fluorescence directly correlates with the suppression efficiency.[34] However, the efficiency of AcdRS A9 was insufficient for the production of artificial photoenzymes containing thioX.

To improve thioX incorporation, we envisioned transforming AcdRS A9 into a thioX-specific synthetase (thioXRS). First, we built a molecular model to guide site-specific mutagenesis, based on the structure of the aaRS G2 complexed with a ncAA (BibaF, PDB entry code 4PBR).[32] We adapted its amino acid sequence in silico to match that of AcdRS A9 by exchanging six amino acids (Table S3) and replacing the ligand with thioX before generating an energy-minimized protein model. Visual inspection identified D65 as a key residue in proximity to thioX (see Figure 2). Since D65 in AcdRS A9 is critical for recognizing the endocyclic nitrogen atom of the Acd side chain, we hypothesized that modifying this position could shift specificity from Acd to thioX. We therefore generated a focused library to fully randomize position 65 via site saturation mutagenesis, employing a primer containing an NNK codon.

Initial screening of the variants was performed in whole cells, co-expressing the sfGFP_S2TAG reporter gene in the presence of thioX. We selected six candidates and further validated them by monitoring the sfGFP fluorescence in the presence and absence of thioX. This approach allowed us to exclude variants that utilize canonical amino acids and revealed the D65W variant as the only improved variant with a twofold increase in suppres-

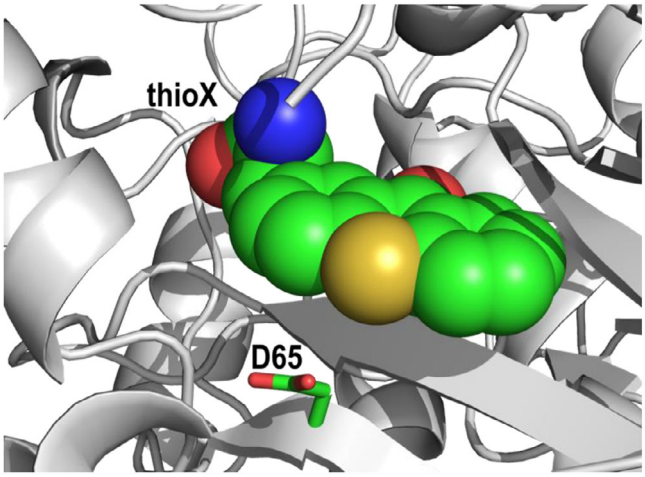

Figure 2. Close-up view of the AcdRS model bound to thioX shown as spheres.

sion efficiency compared to the parental AcdRS (compare Figures S1–S3).

The finding that the sterically demanding tryptophan side chain facilitated the accommodation of the ligand's sulfur atom was initially surprising. We hypothesized that W65 forms a $\pi-\pi$ interaction with the thioxanthone ring of the substrate as it has been seen in AzAlaRS.[35] Titration with thioX-OMe allowed us to find the optimal conditions for incorporating thioX into target proteins. Remarkably, a concentration of 0.25 mM was sufficient to achieve a near-complete suppression efficiency, which was significantly lower than the standard concentration of 1 mM commonly used in established protocols. This minimizes the consumption of precious ncAA and prevents unwanted putative toxicity effects by high thioX concentrations (see Figures S4–S5). In summary, we have developed an efficient system for incorporating thioX through the interplay of aaRS engineering and ncAA derivatization.

2.3. LmrR as Photoenzyme

Following the development of the synthetase thioXRS, we selected LmrR as a protein scaffold to create a novel photoenzyme harboring a thioxanthone moiety. Residues V15, F93, and W96 were initially selected as suitable positions for thioX incorporation. V15 and F93 were recently replaced to accommodate various ncAAs, allowing the creation of catalysts with new-to-nature activities. A *p*-aminophenylalanine (pAF) at position V15 improved the catalytic efficiency of an oxime-forming enzyme.[36] On the other hand, substitution of residue F93 with Bpa[24] and more recently, via bioconjugation to an introduced Cys[20] have led to the creation of different photoenzymes. In addition to these known positions, we targeted residue W96, which typically binds and stabilizes a variety of ligands through $\pi-\pi$ interactions. We envisioned that replacing the native tryptophan with thioX could harness this property to generate an efficient photoenzyme.

Following careful selection of the target positions, we overexpressed the three LmrR variants LmrR_15thioX, LmrR_93thioX, and LmrR_96thioX. They were successfully produced and purified from *E. coli* cell extracts (see Figure S6) for their use in photobiocatalytic reactions. We confirmed the thioX incorporation by MS analysis (see Figure S7), further demonstrating the functionality of the developed thioXRS.

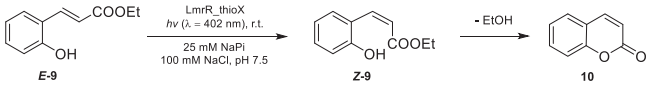

Scheme 1. Model reaction catalyzed by LmrR_thioX variants. Reaction conditions: pH 7.5 (25 mM sodium phosophate buffer, 100 mM NaCl, 100 µM substrate, illumination with a LED with a λ_{max} of 402 nm.

2.4. Performance of LmrR_thioX Variants in a Fluorescence-Based Photoreaction

Thioxanthone is known to act as a sensitizer for the *E*/*Z* isomerization of various fumarate and cinnamate esters and amides.[37,38] To validate the functionality of the LmrR_thioX variants, we investigated their catalytic performance in the isomerization reaction of (*E*)-*o*-hydroxycinnamic acid ethyl ester (*E*-**9**). Excitation of the thioX moiety initiates EnT to *E*-**9**, driving the isomerization to form *Z*-**9**, which subsequently cyclizes to coumarin (**10**) (Scheme 1). The selected model reaction allows real-time monitoring of the conversion by measuring the fluorescence of **9**, which decreases as it is converted to the non-fluorescent product **10**. This direct correlation can be harnessed for reaction engineering and for screening variants with higher catalytic efficiency.

To further qualify the EnT mechanism underlying the photocatalytic activity of thioX on the conversion of *E*-**9** into **10**, a comprehensive spectroscopic analysis was undertaken. From UV-vis absorption, steady-state fluorimetry and time-resolved fluorescence experiments (Figures S8 and S9), we reason that EnT takes place in the form of Förster's resonance energy transfer (FRET).

We evaluated the initial performance of the photoenzyme variants and identified LmrR_96thioX as the most efficient catalyst, achieving nearly complete conversion after 2 h, as determined by fluorescence measurements (Figure 3A). In contrast, the other variants exhibited only moderate conversions of approximately 30%. Similarly, low conversion was observed in a control reaction using an equimolar amount of free TXT as the catalyst. In the absence of light, catalyst, or photoenzyme, only a slight decrease in fluorescence was observed, likely due to direct excitation of *E*-**9** (see Figure S10).

We confirmed the conversion of *E*-**9** to coumarin by HPLC measurements, which correlated well with the fluorescence data set (Figure 3B, see Figures S13–S18 for chromatograms). LmrR_96thioX achieved more than 50% conversion within the first 30 min of reaction (see Figure S11). This demonstrates the improved kinetics of the photoenzyme over the other variants and free TXT. Trace amounts (~5%) of coumarin were already present prior to irradiation, likely as an impurity of the substrate synthesis procedure. To investigate potential inactivation of the photoenzymes through cross-linking, we performed SDS-

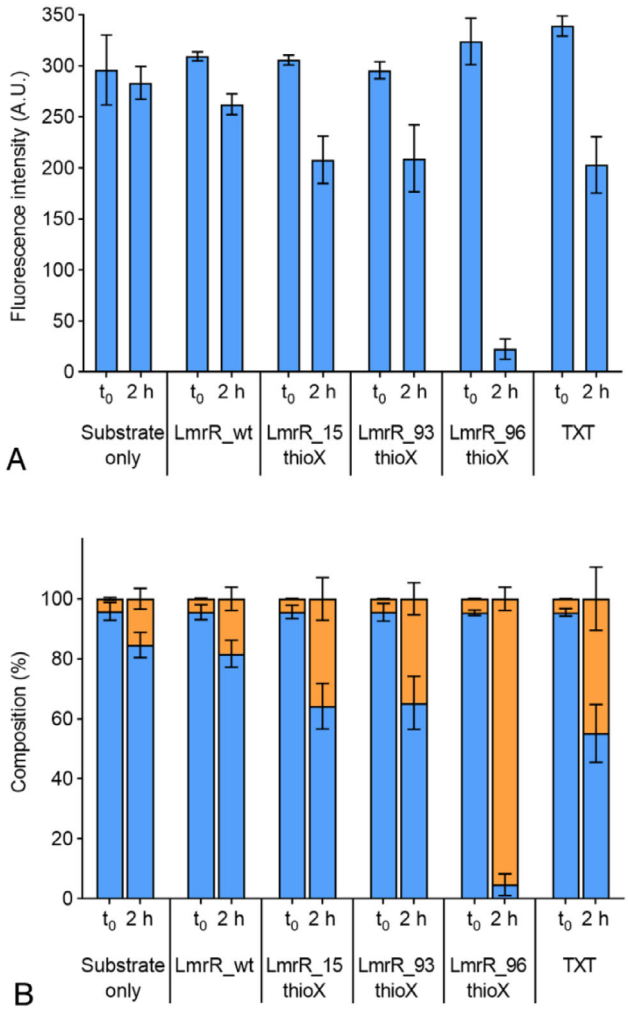

Figure 3. A) Analysis of the photoisomerization reaction by measuring the decreasing fluorescence intensity due to substrate conversion. Reaction conditions: 100 μM *E*-**9**, 2.5 μM LmrR_thioX variant (concentration of the dimer: 1.25 μM), 25 mM sodium phosphate, pH 7.5, irradiation with a 402 nm LED at 25 °C. Fluorescence emission was recorded at 550 nm (excitation at 330 nm). As controls, two reactions were established, one omitting the photoenzyme and one replacing it with TXT (1.25 μM). Results are represented as mean value ± SD of independent replicates ($n = 3$). B) Composition of the photoreactions established by HPLC. For HPLC analysis, peak areas were used to determine the concentration of *E*-**9** and **10** in each sample. Results are represented as mean value ± SD of independent replicates ($n = 3$).

PAGE analysis, which revealed no evidence of intermolecular cross-linking between the two LmrR subunits (data not shown).

Finally, we investigated the kinetic properties of LmrR_96thioX, our most promising candidate. This variant exhibited a K_m of 76 ± 17 μM and a k_{cat} of 0.84 ± 0.24 min^{-1} (see Figure S19). These values are consistent with the behavior observed during the photoreactions, in which full conversion was achieved within 2 h. Although LmrR_96thioX binds *E*-**9** with relatively high affinity, the substrate positioning within the active site might not be optimal for the reaction to happen efficiently. Remarkably, despite no further engineering beyond the incorporation of thioX, LmrR_96thioX displays significant catalytic activity. Further improvements could be achieved by elucidating the binding mode of *E*-**9** and selectively targeting residues within the protein cavity to produce variants with enhanced catalytic efficiency. In summary, we identified LmrR_96thioX as an artificial photoenzyme, capable of catalyzing the light-driven *E*/*Z* isomerization of *E*-**9**, which outperformed both the other variants and free TXT. This confirms the utility of LmrR as a robust photoprotein scaffold, due to its ability to bind compounds with high affinity and to the placement of thioxanthone as photocatalytic cofactor within its central pocket.

3. Conclusion

In this work, we established a versatile tool for the genetic incorporation of the noncanonical amino acid thioX. The synthesis of thioX-OMe provided a practical solution to overcome solubility and bioavailability issues, thereby facilitating the efficient incorporation into proteins. By engineering the AcdRS synthetase, we developed a thioXRS variant with an improved suppression efficiency that allowed the efficient incorporation of thioX under optimized conditions.

To prove the functionality of this system, we generated a photoenzyme, based on the protein scaffold LmrR and identified LmrR_96thioX as the most effective catalyst in the conversion of *E*-**9** to coumarin under visible-light irradiation.

Overall, we have developed a robust system for incorporating thioxanthone into proteins and demonstrated its utility in creating a new-to-nature photoenzyme.

While preparing this manuscript, an alternative thioXRS was published, involving the engineering of a pyrrolysyl-tRNA synthetase in contrast to our tyrosyl-tRNA-synthetase. Chen et al. demonstrated that incorporating thioxanthone enabled the creation of photoenzymes capable of catalyzing a stereoselective [2 + 2] photocycloaddition reaction.[39] Interestingly, Crawshaw et al. reported efficient thioX-based photoenzymes for stereoselective [2 + 2] photocycloadditions and C-H insertions. Like our thioXRS, they succeeded in incorporating thioxanthone using an engineered tyrosyl-tRNA synthetase bearing a tryptophan residue in its active site. Both engineering approaches led to a similar improvement over the identical parental aaRS, despite the different positioning of the tryptophan (L108W).[40] The development of these synthetases as molecular tools, along with their application in engineering different types of photoenzymes, underscores the potential of photobiocatalysis and paves the way for future advancements in the engineering of protein-based photocatalysts.

4. Experimental Section

All constructs generated in this study have been verified by Sanger Sequencing. Plasmids, PCR products and mutagenesis reactions were isolated or purified using NucleoSpin Plasmid (NoLid) kit and NucleoSpin Gel and PCR Clean-up (MACHEREY-NAGEL), respectively. Samples were treated according to manufacturer's instructions except for the elution step which was performed with water. All plasmids, primers, and sequences used in this study are listed in the Supporting Information.

4.1. aaRS Modeling

Starting from the structure of the G2 aaRS from *Methanocaldococcus jannaschii* (PDB entry code 4PBR), the sequence was adapted to that of AcdRS A9. The BibaF ligand was replaced by thioX and an energy minimization protocol in YASARA[41] was applied. Figures were generated using Pymol 1.8.0.2 (Schrödinger, LLC).

4.2. Site-directed Mutagenesis Protocol

Site-directed substitutions and deletions were introduced using a mutagenesis protocol based on the Q5 site-directed mutagenesis kit from New England Biolabs (Frankfurt am Main, Germany). Briefly, after PCR amplification using the desired mutagenic primers, the purified PCR product was diluted in 1x T4 DNA ligase buffer (NEB) and 0.5 µL each of T4 polynucleotide kinase, T4 DNA ligase, and DpnI (NEB) was added (10 µL final volume). Following incubation at room temperature for 15 min, the reaction was further incubated at 37 °C for another 1 h. A volume of 5 µL was transformed into chemically competent *E. coli* TOP10 cells and plated on LB agar containing the appropriate antibiotics.

4.3. thioXRS & GFP Reporter Plasmid Cloning

In this work, the pEVOL plasmid system was used to incorporate thioX.[42] The second gene copy of the BpaRS (under control of the constitutive promoter glnS) in the pEVOL-pBpF plasmid was removed by site-directed mutagenesis using the primer pair MTE013/014 (see protocol above).[43]

The original BpaRS sequence was replaced by that of AcdRS A9 containing the additional D286R mutation to further increase the aminoacylation efficiency.[31,44] This was achieved by overlap-extension PCR, followed by digestion with BglII and SalI (NEB) and subsequent ligation with T4 DNA ligase (NEB). The resulting plasmid (pMTE044) served as template for the thioXRS engineering campaign.

The sfGFP reporter plasmid was constructed by amplification of the sfGFP gene by standard PCR. The S2TAG mutation was introduced by the primer MTE002 carrying the respective nucleotide substitution. The PCR products and pET28 vector were digested with NcoI and XhoI (NEB), purified by gel electrophoresis, and subsequently ligated with T4 DNA ligase (NEB).

Please note that this cloning strategy led to the addition of a glycine residue (see Supporting Information). However, amino acid numbering remained unaffected.

4.4. thioXRS Variant Library Generation

A library targeting residue D65 was generated by PCR using the primer pair MTE028/MTE029 carrying an NNK degenerate codon. Following amplification, 100 ng of the purified PCR product was used as input for the mutagenesis procedure as described above.

To determine the library size, 100 µL of the recovered cells was plated on LB agar containing the appropriate antibiotic (chloramphenicol 34 µg/mL). This procedure yielded a 34-fold library coverage. The remaining recovered cells were used to inoculate a 10 mL LB culture containing the appropriate antibiotic (chloramphenicol 34 µg/mL) and grown overnight at 37 °C. This culture was harvested by centrifugation and the plasmid DNA was isolated. The quality of the generated library was confirmed by Sanger sequencing.

4.5. thioXRS Variant Library Screening

The thioXRS library plasmid (50 ng) was used to transform chemically competent *E. coli* BL21(DE3) cells containing the sfGFP_S2TAG reporter plasmid (pMTE012) and plated on LB agar containing the appropriate antibiotics (kanamycin 50 µg/mL, chloramphenicol 25 µg/mL). The plasmid containing the parental AcdRS A9_D286R (pMTE044) served as control and was treated identically.

From the library plate, 88 single colonies were picked and used to inoculate LB medium with the appropriate antibiotics (kanamycin 50 µg/mL, chloramphenicol 34 µg/mL) in a microtiter plate (MTP) and grown overnight at 37 °C. In addition, 8 single colonies from the parental control plate were picked and processed accordingly.

These overnight cultures were diluted 1:100 into the main culture in a screening deep-well plate (DWP) containing LB medium with kanamycin 25 µg/mL and chloramphenicol 17 µg/mL. Sterile glycerol (21% v/v final concentration) was added to the remaining culture to generate a masterplate, which was then stored at −80 °C. The screening DWP was further incubated for 4 h at 37 °C before adding a 10x inducer mix (10 mM thioX, 10 mM IPTG, 0.2% arabinose in 50% DMSO) to the 88 variants and the 4 parental clones. To the remaining 4 parental clones a 10x inducer mix lacking the ncAA was added, serving as control. The plate was incubated for an additional 18 h at 37 °C under constant shaking (500 rpm). After this, GFP fluorescence was measured as described below. The clones yielding a fluorescence signal higher than the parental control were selected as positive hits.

For detailed hit validation and plasmid isolation, the master plate was used to inoculate an overnight LB culture containing the appropriate antibiotics (kanamycin 50 µg/mL, chloramphenicol 34 µg/mL) and grown overnight at 37 °C. Hits validation followed the same procedure as the initial screening but was carried out in duplicate in the presence and absence of thioX, respectively. In addition, the overnight culture was used to inoculate a 10 mL LB culture (chloramphenicol 34 µg/mL) for plasmid isolation.

To remove the sfGFP_S2TAG reporter plasmid, the isolated plasmids were digested with NaeI (NEB) and subsequently purified. The purified plasmids (1 ng) were transformed into chemically competent *E. coli* TOP10 cells and plated on LB agar with appropriate selection (chloramphenicol 25 µg/mL or kanamycin 50 µg/mL as control to check for residual reporter plasmid). Single colonies were then used to inoculate LB medium and grown overnight at 37 °C. The plasmids were then extracted and verified by Sanger Sequencing.

4.6. thioXRS (D65W variant) Characterization

The plasmid (see Supporting Information for full sequence) encoding the thioXRS D65W variant (pEVOL_thioXRS / pMTE058) was transformed into chemically competent *E. coli* BL21(DE3) cells containing the sfGFP_S2TAG reporter plasmid (pMTE012) and plated on LB agar with appropriate antibiotics (kanamycin 50 µg/mL, chloramphenicol 25 µg/mL). Single colonies were used to inoculate LB medium (kanamycin 50 µg/mL, chloramphenicol 34 µg/mL) in a DWP in triplicates and grown overnight at 37 °C. Subsequently, these cultures were diluted 1:100 into fresh LB medium (kanamycin 25 µg/mL, chloramphenicol 17 µg/mL) and grown for 3.5 h before the addition of 0.02% arabinose and the 0.25 mM of thioX-OMe in DMSO. After 30 min, 1 mM IPTG was added to induce the expression of the sfGFP reporter and the DWP was further grown for 18–20 h at 37 °C. The fluorescence was measured as described below.

4.7. sfGFP Reporter Fluorescence Measurement

Cells were diluted 1:10 into buffer (50 mM sodium phosphate, 150 mM NaCl, pH 8.0) in a black MTP with transparent bottom (Greiner Bio-One). OD_{600} and fluorescence (λ_{Ex} 460 nm, λ_{Em} 510 nm) were measured on an Infinite 200 Pro Tecan plate reader. For the analysis, fluorescence values were normalized by the corresponding OD_{600}.

4.8. LmrR Expression, Purification, and Analysis

BL21(DE3) cells containing the plasmid pEVOL_thioXRS (pMTE058) were transformed with the plasmids encoding LmrR_wt, LmrR_V15TAG, LmrR_F93TAG or LmrR_W96TAG and plated on LB agar with the appropriate antibiotics (kanamycin 50 μg/mL, chloramphenicol 25 μg/mL). Single colonies of each transformation were grown overnight at 37 °C in 4 mL cultures with appropriate antibiotics (kanamycin 50 μg/mL, chloramphenicol 34 μg/mL). Each culture was diluted 1:100 into a 50 mL auto induction medium[45] culture (kanamycin 25 μg/mL, chloramphenicol 17 μg/mL) containing 0.25 mM thioX-OMe and grown at 37 °C for 3–4 h. After this, the temperature was switched to 30 °C and the cultures were grown for another 19–20 h. Cells were harvested by centrifugation at 4500 x *g* for 20 min and resuspended in 100 mM Tris-HCl, 150 mM NaCl buffer at pH 8. To this suspension, 0.1% Triton-X100 and 1 mg/mL lysozyme were added, and the mixture was incubated at 4 °C for 2 h with occasional inversion. Subsequently, cells were disrupted by ultrasonication (30 sec, 5 × 10 cycle, 50% power) and centrifuged at 10,000 x *g* and 4 °C for 30 min. The clarified lysates were applied to a Strep-Tactin XT resin (IBA lifesciences), and proteins were eluted following the manufacturer´s instructions (binding and washing buffer: 100 mM Tris-HCl, 150 mM NaCl, pH 8; elution buffer: 100 mM Tris-HCl, 150 mM NaCl, 50 mM Biotin, pH 8).

After purification, the buffer was exchanged (25 mM sodium phosphate, 100 mM NaCl, pH 7.5) and the protein was concentrated using an Amicon Ultra centrifugal filter (10.000 MWCO, Merck Millipore). Protein concentration was determined using a Nanodrop spectrophotometer (Thermo Fisher Scientific).

4.9. MS Analysis of LmrR_thioX Variants

Protein samples were diluted to a final concentration of 0.1–0.2 mg/mL in buffer (50 mM sodium phosphate, 250 mM NaCl, pH 7.0) and analyzed using an Agilent 1260 Infinity LC system coupled to an Agilent 6530 Accurate-Mass Q-TOF MS (Agilent Technologies). Separation was performed on a ProntoSIL C4 column (100 × 2.0 mm, 5 μm; Bischoff Chromatography) using a linear gradient of 5–100% ACN over 20 min at a flow rate of 0.5 mL/min. Mass spectra were acquired and deconvoluted using the maximum entropy algorithm, across a mass range of 10–40 kDa.

4.10. Photoreactions with LmrR_thioX Variants

A photoreactor was built according to a published model.[46] A single LED (TRU COMPONENTS YDG-504VC, 402 nm) was inserted into the cap of a 2 mL glass vial and controlled by an Arduino Microcontroller. Photoreactions were carried out in triplicate using 2.5 μM of the purified LmrR_thioX variants and 100 μM of the substrate *E*-**9** in buffer (25 mM sodium phosphate, 100 mM NaCl, pH 7.5). As controls, photoreactions containing only the substrate, LmrR_wt or the free TXT (1.25 μM) as catalysts were established. All photoreactions were irradiated with a single LED (402 nm) at 25 °C under constant stirring for a total time of 2 h. To monitor the reaction progress, aliquots were taken at different time points (0, 30, and 120 min) and immediately stored at −20 °C. As a nonirradiated control, one aliquot was taken and kept in the dark. All samples were processed and analyzed simultaneously.

4.11. Fluorescence Measurement and HPLC Analysis

Samples were diluted with an equal volume of ACN and incubated at 30 °C under shaking (900 rpm) for 1 h. Following incubation, they were centrifuged at 3000 × *g* and room temperature for 10 min. For fluorescence measurement, the supernatant was diluted in 10% ACN/H_2O into a black MTP (Greiner Bio-One) and measured on an Infinite 200 Pro Tecan plate reader (λ_{Ex} 330 nm, λ_{Em} 550 nm). For HPLC analysis, the supernatant was injected into a 1260 Infinity II LC system (Agilent Technologies) equipped with a Luna Omega 5 μm Polar C18 100 Å LC column (150 × 4.6 mm; Phenomenex). To quantify *E*-**9** and **10**, calibration curves ranging from 100 μM to 1.56 μM were generated in triplicate.

4.12. LmrR_96thioX kinetics

The kinetic parameters of LmrR_96thioX were determined as follows. Photoreactions were carried out in triplicates using 1 μM of the purified LmrR_96thioX and various concentrations of *E*-**9** (0, 25, 50, 75, 100, 125, 150, 200, 250, and 300 μM) in buffer (25 mM sodium phosphate, 100 mM NaCl, pH 7.5). Reactions were performed as described above and samples were taken every 5, 10, 15, 20, 25, and 30 min by sampling 50 μL of the reaction and quenching with an equal volume of ACN. Samples were treated accordingly before being injected into a 1260 Infinity II LC system (Agilent Technologies) equipped with a Luna Omega 5 μm Polar C18 100 Å LC column (150 × 4.6 mm; Phenomenex).

4.13. Fluorescence Decay Measurements

The decays were recorded in time-correlated single-photon counting (TCSPC) mode using a setup which is extensively described elsewhere.[47,48] Briefly, picosecond laser pulses are delivered to the sample and the fluorescence is collected at 90° to the excitation beam through a 20X microscope objective. The latter is equipped with a >430 nm long-wavelength pass filter (Semrock) rejecting residual excitation stray light and focuses the fluorescence photons onto the sensitive area of a single-photon avalanche diode (model PCM50, Micro Photon Devices). The avalanche photocurrent pulses serve as the STOP signal to an integrated TCSPC PC board (SPC150, Becker & Hickl), synchronized with the laser pulses. In this work, we used as the laser source a BDS-SM-405 diode laser emitting 35 ps pulses at 405 nm with repetition rate set at 20 MHz (Becker & Hickl). The pure substrate sample was excited using the third harmonic at 355 nm, generated out of cavity according to a previously reported procedure[47] of a GE100 Nd:VAN cw-mode-locked laser (Time Bandwidth Products).

The fluorescence decay distributions were fitted to multi-exponential decay functions over a constant background, applying the Levenberg-Marquardt χ^2 minimization algorithm implemented within the data analysis software origin 2024. Ten decay distributions were acquired for each sample. The errors reported in Table S1 are the standard deviations of the fitting parameters retrieved in homologous decays.

Acknowledgments

M.H. has received funding from the European Research Council (ERC) under the European Union's Horizon 2020 research and innovation programme (grant agreement No. 759262). The pEVOL-pBpF plasmid was a kind gift from Peter Schultz (Addgene plasmid # 31190). The authors would like to thank Uwe Bornscheuer for providing laboratory space and equipment, as well as for his helpful discussions throughout the course of this work. We also gratefully acknowledge Hannes Meinert for his assistance in establishing the analytical methods and Markus Averbeck for measuring the MS spectra of the LmrR_thioX variants. Finally, we would like to thank Fabian Bock for his insightful discussions and Anton Meier for his contribution to the LightZyme project.

Open access funding enabled and organized by Projekt DEAL.

Conflict of Interests

The authors declare no conflict of interest.

Data Availability Statement

The data that support the findings of this study are available in the supplementary material of this article.

Keywords: Genetic code engineering · New-to-nature · Non-canonical amino acids · Photobiocatalysis · Thioxanthone

[1] M. A. Emmanuel, S. G. Bender, C. Bilodeau, J. M. Carceller, J. S. DeHovitz, H. Fu, Y. Liu, B. T. Nicholls, Y. Ouyang, C. G. Page, T. Qiao, F. C. Raps, D. R. Sorigué, S.-Z. Sun, J. Turek-Herman, Y. Ye, A. Rivas-Souchet, J. Cao, T. K. Hyster, *Chem. Rev.* **2023**, *123*, 5459–5520.
[2] D. Sorigué, B. Légeret, S. Cuiné, S. Blangy, S. Moulin, E. Billon, P. Richaud, S. Brugière, Y. Couté, D. Nurizzo, P. Müller, K. Brettel, D. Pignol, P. Arnoux, Y. Li-Beisson, G. Peltier, F. Beisson, *Science* **2017**, *357*, 903–907.
[3] W. Zhang, M. Ma, M. M. E. Huijbers, G. A. Filonenko, E. A. Pidko, M. van Schie, S. de Boer, B. O. Burek, J. Z. Bloh, W. J. H. van Berkel, W. A. Smith, F. Hollmann, *J. Am. Chem. Soc.* **2019**, *141*, 3116–3120.
[4] G. Londi, G. Salvadori, P. Mazzeo, L. Cupellini, B. Mennucci, *JACS Au* **2025**, *5*, 158–168.
[5] S. Ju, D. Li, B. K. Mai, X. Liu, A. Vallota-Eastman, J. Wu, D. L. Valentine, P. Liu, Y. Yang, *Nat. Chem.* **2024**, *16*, 1339–1347.
[6] V. Tseliou, L. Kqiku, M. Berger, F. Schiel, H. Zhou, G. J. Poelarends, P. Melchiorre, *Nature* **2024**, *634*, 848–854.
[7] F. Cheng, H. Li, D.-Y. Wu, J.-M. Li, Y. Fan, Y.-P. Xue, Y.-G. Zheng, *Green Chem.* **2020**, *22*, 6815–6818.
[8] J. Xu, Y. Hu, J. Fan, M. Arkin, D. Li, Y. Peng, W. Xu, X. Lin, Q. Wu, *Angew. Chem., Int. Ed.* **2019**, *58*, 8474–8478.
[9] J. Li, Y. Ma, N. Liu, B. E. Eser, Z. Guo, P. R. Jensen, G. Stephanopoulos, *Nat. Commun.* **2020**, *11*, 6198.
[10] Z. Qin, Y. Zhou, Z. Li, M. Höhne, U. T. Bornscheuer, S. Wu, *Angew. Chem. Int. Ed.* **2024**, *63*, e202314566.
[11] V. Alphand, W. J. H. van Berkel, V. Jurkaš, S. Kara, R. Kourist, W. Kroutil, F. Mascia, M. M. Nowaczyk, C. E. Paul, S. Schmidt, J. Spasic, P. Tamagnini, C. K. Winkler, *ChemPhotoChem* **2023**, *7*, e202200325.
[12] J.-P. Wang, M.-H. Zong, N. Li, *Chem. Catal.* **2024**, *4*, 100933.
[13] N. A. W. de Kok, S. Schmidt, *Chem. Catal.* **2023**, *3*, 100493.
[14] X. Liu, F. Kang, C. Hu, L. Wang, Z. Xu, D. Zheng, W. Gong, Y. Lu, Y. Ma, J. Wang, *Nature Chem.* **2018**, *10*, 1201–1206.
[15] J. Lee, W. J. Song, *J. Am. Chem. Soc.* **2023**, *145*, 5211–5221.
[16] A. S. Klein, F. Leiss-Maier, R. Mühlhofer, B. Boesen, G. Mustafa, H. Kugler, C. Zeymer, *J. Am. Chem. Soc.* **2024**, *146*, 25976–25985.
[17] M. Bratovič, *Nat. Chem. Biol.* **2024**, *20*, 1387–1387.
[18] J. S. Trimble, R. Crawshaw, F. J. Hardy, C. W. Levy, M. J. B. Brown, D. E. Fuerst, D. J. Heyes, R. Obexer, A. P. Green, *Nature* **2022**, *611*, 709–714.
[19] Y. Fu, X. Liu, Y. Xia, X. Guo, J. Guo, J. Zhang, W. Zhao, Y. Wu, J. Wang, F. Zhong, *Chem* **2023**, *9*, 1897–1909.
[20] J. Guo, J. Qian, D. Cai, J. Huang, X. Yang, N. Sun, J. Zhang, T. Pang, W. Zhao, G. Wu, X. Chen, F. Zhong, Y. Wu, *J. Am. Chem. Soc.* **2024**, *146*, 19030–19041.
[21] T. Kuckhoff, R. C. Brewster, C. T. J. Ferguson, A. G. Jarvis, *Eur. J. Org. Chem.* **2023**, *26*, e202201412.
[22] Y. Gu, K. Ellis-Guardiola, P. Srivastava, J. C. Lewis, *ChemBioChem* **2015**, *16*, 1880–1883.
[23] B. Brouwer, F. Della-Felice, J. H. Illies, E. Iglesias-Moncayo, G. Roelfes, I. Drienovská, *Chem. Rev.* **2024**, *124*, 10877–10923.
[24] N. Sun, J. Huang, J. Qian, T.-P. Zhou, J. Guo, L. Tang, W. Zhang, Y. Deng, W. Zhao, G. Wu, R.-Z. Liao, X. Chen, F. Zhong, Y. Wu, *Nature* **2022**, *611*, 715–720.
[25] N. F. Nikitas, P. L. Gkizis, C. G. Kokotos, *Org. Biomol. Chem.* **2021**, *19*, 5237–5253.
[26] G. Roelfes, *Acc. Chem. Res.* **2019**, *52*, 545–556.
[27] J. K. Takimoto, Z. Xiang, J.-Y. Kang, L. Wang, *ChemBioChem* **2010**, *11*, 2268–2272.
[28] H. Zhou, J. W. Cheung, T. Carpenter, S. K. Jones, N. H. Luong, N. C. Tran, S. E. Jacobs, S. A. Galbada Liyanage, T. A. Cropp, J. Yin, *Bioorg. Med. Chem. Lett.* **2020**, *30*, 126876.
[29] I. N. Arthur, J. E. Hennessy, D. Padmakshan, D. J. Stigers, S. Lesturgez, S. A. Fraser, M. Liutkus, G. Otting, J. G. Oakeshott, C. J. Easton, *Chem. - Eur. J.* **2013**, *19*, 6824–6830.
[30] L. C. Speight, A. K. Muthusamy, J. M. Goldberg, J. B. Warner, R. F. Wissner, T. S. Willi, B. F. Woodman, R. A. Mehl, E. J. Petersson, *J. Am. Chem. Soc.* **2013**, *135*, 18806–18814.
[31] I. Sungwienwong, Z. M. Hostetler, R. J. Blizzard, J. J. Porter, C. M. Driggers, L. Z. Mbengi, J. A. Villegas, L. C. Speight, J. G. Saven, J. J. Perona, R. M. Kohli, R. A. Mehl, E. J. Petersson, *Org. Biomol. Chem.* **2017**, *15*, 3603–3610.
[32] R. B. Cooley, P. A. Karplus, R. A. Mehl, *ChemBioChem* **2014**, *15*, 1810–1819.
[33] W. N. Zagotta, B. S. Sim, A. K. Nhim, M. M. Raza, E. G. Evans, Y. Venkatesh, C. M. Jones, R. A. Mehl, E. J. Petersson, S. E. Gordon, *eLife* **2021**, *10*, e70236.
[34] A. Tuley, Y.-S. Wang, X. Fang, Y. Kurra, Y. H. Rezenom, W. R. Liu, *Chem. Commun.* **2014**, *50*, 2673–2675.
[35] T. Baumann, M. Hauf, F. Schildhauer, K. B. Eberl, P. M. Durkin, E. Deniz, J. G. Löffler, C. G. Acevedo-Rocha, J. Jaric, B. M. Martins, H. Dobbek, J. Bredenbeck, N. Budisa, *Angew. Chem., Int. Ed.* **2019**, *58*, 2899–2903.
[36] I. Drienovská, C. Mayer, C. Dulson, G. Roelfes, *Nature Chem.* **2018**, *10*, 946–952.
[37] M. Suga, S. Fukushima, K. Makino, K. Nakamura, H. Tabata, T. Oshitari, H. Natsugari, N. Kuroda, K. Kanemaru, Y. Oda, H. Takahashi, *J. Org. Chem.* **2024**, *89*, 8836–8844.
[38] T. Neveselý, J. J. Molloy, C. McLaughlin, L. Brüss, C. G. Daniliuc, R. Gilmour, *Angew. Chem., Int. Ed.* **2022**, *61*, e202113600.
[39] K.-Y. Chen, H. Ming, H.-X. Wang, H.-Q. Wang, Z. Xiang, *Angew. Chem., Int. Ed.* **2025**, *64*, e202419022.
[40] R. Crawshaw, R. Smithson, J. Hofer, F. J. Hardy, G. W. Roberts, J. S. Trimble, A. R. Kohn, C. W. Levy, D. A. Drost, C. Merten, D. J. Heyes, R. Obexer, T. Bach, A. P. Green, *Nat. Chem.* **2025**, *17*, 1083–1090.
[41] E. Krieger, G. Koraimann, G. Vriend, *Proteins Struct. Func. Bioinf.* **2002**, *47*, 393–402.
[42] T. S. Young, I. Ahmad, J. A. Yin, P. G. Schultz, *J. Mol. Biol.* **2010**, *395*, 361–374.
[43] J. W. Chin, A. B. Martin, D. S. King, L. Wang, P. G. Schultz, *Proc. Natl. Acad. Sci. USA* **2002**, *99*, 11020–11024.

[44] T. Kobayashi, O. Nureki, R. Ishitani, A. Yaremchuk, M. Tukalo, S. Cusack, K. Sakamoto, S. Yokoyama, *Nat. Struct. Mol. Biol.* **2003**, *10*, 425–432.
[45] C. J. Taylor, F. J. Hardy, A. J. Burke, R. M. Bednar, R. A. Mehl, A. P. Green, S. L. Lovelock, *Protein Sci.* **2023**, *32*, e4640.
[46] Z. C. Litman, Y. Wang, H. Zhao, J. F. Hartwig, *Nature* **2018**, *560*, 355–359.
[47] M. Lamperti, A. Maspero, H. H. Tønnesen, M. Bondani, L. Nardo, *Molecules* **2014**, *19*, 13282–13304.
[48] L. Nardo, A. Maspero, A. Penoni, G. Palmisano, E. Ferrari, M. Saladini, *PLoS One* **2017**, *12*, e0175225.

Manuscript received: May 9, 2025
Revised manuscript received: July 22, 2025
Accepted manuscript online: July 28, 2025
Version of record online: August 19, 2025